Cosmological Inflation in N-Dimensional Gaussian Random Fields with Algorithmic Data Compression

Connor A. Painter and Emory F. Bunn
Physics Department, University of Richmond, Richmond, VA 23173, USA

The leading modern theories of cosmological inflation are increasingly multi-dimensional. The "inflaton field" $\boldsymbol{\phi}$ that has been postulated to drive accelerating expansion in the very early universe has a corresponding potential function V, the details of which, such as the number of dimensions and shape, have yet to be specified. We consider a natural hypothesis that V ought to be maximally random. We realize this idea by defining the V as a Gaussian random field in some number N of dimensions. We repeatedly simulate of the evolution of $\boldsymbol{\phi}$ given a set of conditions on the "landscape" of V. We simulate a "path" stepwise through $\boldsymbol{\phi}$-space while simultaneously computing V and its derivatives along the path via a constrained Gaussian random process, incorporating the information from prior steps. When N is large, this method significantly reduces computational load as compared to methods which generate the potential landscape all at once. Even so, computation of the covariance matrix $\boldsymbol{\Gamma}$ of constraints on V can quickly become intractable. Inspired by this problem, we present data compression algorithms to prioritize the necessary information already simulated, then keep an arbitrarily large portion. Information such as the evolution of the scale factor and tensor and scalar perturbations can be extracted from any particular path, then statistical information about these quantities can be gathered from repeated trials. In these ways, we present a versatile multi-variable program for exploration into how accurately this emergent model can fit to observation.

I. INTRODUCTION

Characterization of plausible inflationary models is an extremely high priority in cosmology. Since inflationary theory was developed in the late 1970s and 80s, the cosmological community has sought to constrain its main free parameter: the inflaton potential V. There now exist *libraries* of invented potentials which have been exhaustively simulated with various initial conditions in efforts to gauge how accurately each of their predictions align with modern cosmological data. Some model potentials have been shown to be ineffective representatives of the early universe, while a surprising number reliably produce predictions that fall within present uncertainties. A large number of potential candidates have been catalogued, yet only a fraction of parameter space has been sampled. Potentials with high numbers of degrees of freedom N have recently been motivated by developments in string theory, but come with computational challenges and are often reduced to lower dimensions in favor of more resolved solutions to equations of motion. Furthermore, when V is assumed to be a Gaussian random field, somewhat naturally motivated by CMB observations, high N simulations are extremely intensive due to complicated correlations that scale with N^2 and the resolution.

In the following sections, we motivate and present methods for exploration into the Gaussian random potential model, including data compression algorithms that may make higher degrees of freedom more attainable, as well as preliminary findings from our own supercomputer simulations. The paper is structured as follows: *clarify once more sections are filled in.*

A. Multi-field Inflation

As customary in inflationary theory, we suppose there existed some "inflaton" field $\boldsymbol{\phi}(t, \boldsymbol{x})$ which permeated the early universe with time evolution was governed by its associated potential function $V(\boldsymbol{\phi})$. We assume that the inflaton field was approximately homogeneous in space with small perturbations, i.e. $\boldsymbol{\phi}(t, \boldsymbol{x}) \approx \boldsymbol{\phi}(t) + \delta\boldsymbol{\phi}(t, \boldsymbol{x})$ In general, $\boldsymbol{\phi} = (\phi^{(0)}, \phi^{(1)}, ..., \phi^{(N-1)})$ is a vector of N components while V is scalar-valued. In addition to its existence, we assert that the inflaton potential dominates the energy density of the early universe so that its characteristics may determine the particularities of large-scale cosmic expansion in early times. The Klein—Gordon equation for the evolution of $\boldsymbol{\phi}$ in terms of V is

$$\ddot{\boldsymbol{\phi}} + 3H\dot{\boldsymbol{\phi}} + \nabla_\phi V = 0 \tag{1}$$

where overdots signify derivatives with respect to cosmic time t, H is the Hubble parameter, and Planck units $c = \hbar = 8\pi G = 1$ are implemented throughout. H is related to the field and its potential by the Friedmann Equation,

$$3H^2 = \frac{1}{2}\left|\dot{\boldsymbol{\phi}}\right|^2 + V \tag{2}$$

Component-wise, (1) reads

$$\ddot{\phi}^{(\alpha)} + 3H\dot{\phi}^{(\alpha)} + \frac{\partial V}{\partial \phi^{(\alpha)}} = 0 \tag{3}$$

where $\alpha = 0, 1, ..., N-1$. This equation recalls the familiar intuition of a ball rolling around on a surface with friction, an analogy we can carry with us through this paper. If $\boldsymbol{\phi}$ locates the ball in N-dimensional space, and $V(\boldsymbol{\phi})$ locates an additional height, then the ball

accelerates *downhill* in response to slopes $\nabla_\phi V$, but is resisted by a frictional term $3H\dot{\boldsymbol{\phi}}$.

In practice, it is often useful to measure time in terms of the expansion of the universe [3]. During inflation, the scale factor $a(t)$ is theorized to have grown exponentially, so a natural unit of time is the "number of e-folds"

$$N_e(t) = \ln\left(\frac{a(t)}{a(t_i)}\right) \tag{4}$$

where t_i is some arbitrary start time of inflation. Some algebra transforms (3) into

$$\frac{d^2\phi^{(\alpha)}}{dN_e^2} + (3-\epsilon)\frac{d\phi^{(\alpha)}}{dN_e} + \frac{1}{H^2}\frac{\partial V}{\partial \phi^{(\alpha)}} = 0 \tag{5}$$

in which we have defined the slow-roll parameter ϵ as

$$\epsilon \equiv -\frac{\dot{H}}{H^2} = \frac{1}{2}\left|\frac{d\boldsymbol{\phi}}{dN_e}\right|^2, \tag{6}$$

signaling the end of inflation at t_e when $\epsilon \uparrow 1$. Note that H can be computed at any time step by

$$H^2 = \frac{V}{3-\epsilon} \tag{7}$$

Given some reasonable model potential, the second-order differential equation (5) can be solved numerically with initial conditions $\boldsymbol{\phi}_i = \boldsymbol{\phi}(t_i)$ and $\dot{\boldsymbol{\phi}}_i = \dot{\boldsymbol{\phi}}(t_i)$. Often times, the initial rate of change is set to slow roll equilibrium so that $\ddot{\boldsymbol{\phi}}_i = 0$. By (1), the approximation is

$$\dot{\boldsymbol{\phi}}_i = H_i\frac{d\boldsymbol{\phi}_i}{dN_e} \approx -\frac{\nabla_\phi V_i}{3H_i}. \tag{8}$$

Furthermore, if $|\dot{\boldsymbol{\phi}}|^2$ is assumed to be negligibly small, then (2) reduces to $3H^2 \approx V$ and the slow-roll approximation is

$$\frac{d\boldsymbol{\phi}_i}{dN_e} \approx -\frac{\nabla_\phi V_i}{V_i} \tag{9}$$

From this point, numerical integration can solve for the inflaton field evolution $\boldsymbol{\phi}(t)$ until $\epsilon \uparrow 1$. Once integration finishes, the values of $\boldsymbol{\phi}$, $\dot{\boldsymbol{\phi}}$, V, $\nabla_\phi V$, ϵ, and H are known at discrete times between t_i and t_e. We refer to this set of information as the inflaton field *trajectory*.

B. Power Spectra

Various observable quantities can be extracted from the trajectory, such as the power spectra of adiabatic curvature (matter) fluctuations $\mathscr{P}_S$ and tensor fluctuations $\mathscr{P}_T$, and the non-Gaussianity of the CMB. In this paper, we will focus on the power spectra.

Following [3], matter perturbations evolve with the mode matrix $\boldsymbol{\psi}$, an expansion of the comoving fluctuations $\delta\boldsymbol{\phi}$ in the inflaton field. For any given mode k, the mode matrix obeys

$$\frac{d^2\boldsymbol{\psi}}{dN_e^2} + (1-\epsilon)\frac{d\boldsymbol{\psi}}{dN_e} + \left(\frac{k^2}{a^2H^2} - 2 + \epsilon\right)\boldsymbol{\psi} + \boldsymbol{C}\boldsymbol{\psi} = 0 \tag{10}$$

where the coupling matrix $\boldsymbol{C}$ is defined as

$$C^{(\alpha\beta)} = \frac{1}{H^2}\left(\frac{d\phi^{(\alpha)}}{dN_e}\frac{\partial V}{\partial\phi^{(\beta)}} + \frac{d\phi^{(\beta)}}{dN_e}\frac{\partial V}{\partial\phi^{(\alpha)}} + \frac{\partial^2 V}{\partial\phi^{(\alpha)}\partial\phi^{(\beta)}}\right) + (3-\epsilon)\frac{d\phi^{(\alpha)}}{dN_e}\frac{d\phi^{(\beta)}}{dN_e}. \tag{11}$$

Given conditions on $\boldsymbol{\psi}$ and $d\boldsymbol{\psi}/dN_e$ at t_i, equation (10) can be solved numerically up through t_e. At any given time, $\mathscr{P}_S(k)$ is computed as

$$\mathscr{P}_S(k) = \frac{k^3}{2\pi^2}\frac{1}{a^2}\boldsymbol{\Psi}\boldsymbol{\Psi}^\star \tag{12}$$

where $\boldsymbol{\Psi} = \boldsymbol{\psi}\cdot\dot{\boldsymbol{\phi}}/|\dot{\boldsymbol{\phi}}|$ and $\star$ is the conjugate transpose. To be clear, the power spectrum, as with the mode matrix, is a function of both wavenumber and time. We are interested in the shape of $\mathscr{P}_S(k)$ at the end of inflation, as this spectrum will most closely resemble modern observed data. At t_e, we expect it to resemble a power law of amplitude A_S and index n_S around the pivot scale $k_0 = 0.05$ Mpc^{-1}:

$$\mathscr{P}_S(k)\Big|_{t_e} \approx A_S\left(\frac{k}{k_0}\right)^{n_S-1} \tag{13}$$

For any reasonable inflationary model, $\mathscr{P}_S$ can be evolved through time at several modes around k_0 via (10), then fit to (13) at t_e. The best fit parameters A_S and n_S can then be used to gauge the viability and predictive power of the choice of inflaton potential and initial conditions.

Following [2], the power spectrum of tensor perturbations is surprisingly easy to compute:

$$\mathscr{P}_T(k) = \frac{2}{\pi^2}H(t(k))^2. \tag{14}$$

The one-to-one and onto function $t(k)$ yields the time at which a scale of magnitude k last exited the horizon, most easily expressed as its inverse, $k(t) = a(t)H(t)$. Thus, in this definition, $\mathscr{P}_T(k)$ gives by default the power at the end of inflation. As with the matter spectrum, the tensor spectrum can be sampled at several wavenumbers around k_0 and fit to another anticipated power law,

$$\mathscr{P}_T(k) \approx A_T\left(\frac{k}{k_0}\right)^{n_T}. \tag{15}$$

Often times, the tensor perturbations are encapsulated in the tensor-to-scalar ratio r, which is defined naturally

Quantity	Constraint
$\log(10^{10}A_S)$	3.040 ± 0.016
n_S	0.9626 ± 0.0057
$r(k_t)$	< 0.1

TABLE I. Planck constraints on matter and tensor fluctuations.

as the power law ratio for any given k,

$$r(k) = \frac{\mathscr{P}_T(k)}{\mathscr{P}_S(k)} = \frac{A_T}{A_S} \cdot \left(\frac{k}{k_0}\right)^{n_T - n_S + 1}. \tag{16}$$

The tensor-to-scalar ratio is most easily constrained at a scale $k_t = 0.002$ Mpc^{-1}.

Constraints on A_S, n_S, and $r(k_t)$ have been found by recent Planck missions and are summarized in I B [1].

II. FORMALISM

The review in Section I was independent of the inflaton potential, but a definition of $V(\boldsymbol{\phi})$ is the heart of every inflationary model. In this paper, we assume that $V(\boldsymbol{\phi})$ is an N-dimensional Gaussian random field with mean zero, coherence scale s, and energy scale $V_\star$. We detail the intuition behind all three parameters below:

- The coherence scale s is a cutoff distance in $\boldsymbol{\phi}$-space before which values of V are expected to be correlated. If $\boldsymbol{\phi}_i$ is separated from $\boldsymbol{\phi}_j$ by exactly s, then $\Gamma^{(ij)}/V_\star^2 \sim 0.6$, i.e., there is moderate correlation. Random potentials with high s are "stretched" horizontally, take longer to evolve, and accrue more e-folds of inflation.
- The inflationary energy scale $V_\star$ is another standard deviation, but in values of V. For the very first point generated at $\boldsymbol{\phi}_0$, it turns out that $V(\boldsymbol{\phi}_0) \sim \mathcal{N}(0, V_\star^2)$. Current observations suggest the energy scale of inflation is about $V_\star \sim 10^{-5}\ E_{\rm Pl}^4$. *Ted will clarify/elaborate just a touch here.*
- The number of inflaton fields N, or the dimension of V, is a rather interesting and unexplored parameter. Not all inflationary models generalize well to $N > 1$, but Gaussian random fields do so effortlessly.

A. Generating Correlated Points

There are two reasonable ways to generate Gaussian random fields for numerically solving Equation (5): (1) randomly generate many discrete points in an N-dimensional volume, then interpolate between them, or (2) only generate a new point exactly where and when you need it, particularly at each location along the path evolution of $\boldsymbol{\phi}$. The latter method is much more computationally efficient for numerically solving equations of motion: it automatically adjusts in resolution for different $\boldsymbol{\phi}$-scales of interest, does not limit the solution to a certain domain, does not contain extra information which can become extremely burdensome when N becomes large. We describe and implement this method of simulating V—along the path of $\boldsymbol{\phi}$—in the following sections.

Generating points on a Gaussian random field is a constrained random process; every new point is generated randomly *constrained by* every previously generated point. This is necessary to maintain that the field be continuous and (infinitely) differentiable. Suppose that V is known at sequence of o points $\boldsymbol{\phi}_0, \boldsymbol{\phi}_1, \ldots, \boldsymbol{\phi}_{o-1}$, and group those values in a vector $\boldsymbol{v}_{\mathscr{O}}$. Now, we want to know V at n new points $\boldsymbol{\phi}_o, \boldsymbol{\phi}_{o+1}, \ldots, \boldsymbol{\phi}_{o+n-1}$, and we call those unknown values $\boldsymbol{v}_{\mathscr{N}}$. First, we need to define the *covariance matrix* $\boldsymbol{\Gamma}$ of constraints on V as an $(o+n) \times (o+n)$ matrix populated with the following correlations,

$$\Gamma^{(ij)} = \langle V(\boldsymbol{\phi}_i) V(\boldsymbol{\phi}_j) \rangle \equiv \langle V_i V_j \rangle \tag{17}$$

$$\langle V_i V_j \rangle = V_\star^2 \exp\left(- \frac{|\boldsymbol{\phi}_i - \boldsymbol{\phi}_j|^2}{2s^2} \right). \tag{18}$$

This symmetric, positive-definite matrix is then broken up into blocks corresponding to the type of information stored,

$$\boldsymbol{\Gamma} = \begin{bmatrix} \boldsymbol{\Gamma}_{\mathscr{O}\mathscr{O}} & \boldsymbol{\Gamma}_{\mathscr{O}\mathscr{N}} \\ \boldsymbol{\Gamma}_{\mathscr{N}\mathscr{O}} & \boldsymbol{\Gamma}_{\mathscr{N}\mathscr{N}} \end{bmatrix}, \tag{19}$$

where $\mathscr{O}$ abbreviates "old" data and $\mathscr{N}$ abbreviates "new" data. Notice that the correlations between all old points are contained in upper-left block, $\boldsymbol{\Gamma}_{\mathscr{O}\mathscr{O}} = \langle \boldsymbol{v}_{\mathscr{O}} \boldsymbol{v}_{\mathscr{O}}^T \rangle$, while correlations between new points are in the lower-right, $\boldsymbol{\Gamma}_{\mathscr{N}\mathscr{N}} = \langle \boldsymbol{v}_{\mathscr{N}} \boldsymbol{v}_{\mathscr{N}}^T \rangle$, and cross correlations are contained in $\boldsymbol{\Gamma}_{\mathscr{N}\mathscr{O}} = \boldsymbol{\Gamma}_{\mathscr{O}\mathscr{N}}^T = \langle \boldsymbol{v}_{\mathscr{N}} \boldsymbol{v}_{\mathscr{O}}^T \rangle$. Since covariances are functions of known distances between points, $\boldsymbol{\Gamma}$ can be populated and used to randomly generate $\boldsymbol{v}_{\mathscr{N}}$. Every value $v_{\mathscr{N}}^{(i)}$ can be considered the sum of the mean $\mu^{(i)}$, as predicted by $\boldsymbol{\Gamma}$, and some constrained random skew $\sigma^{(i)}$. All predicted means are found in the mean vector $\boldsymbol{\mu}$,

$$\boldsymbol{\mu} = \boldsymbol{\Gamma}_{\mathscr{N}\mathscr{O}} \boldsymbol{\Gamma}_{\mathscr{O}\mathscr{O}}^{-1} \boldsymbol{v}_{\mathscr{O}}. \tag{20}$$

The random skews are simultaneously sampled from a multivariate Gaussian distribution of mean zero and covariance $\boldsymbol{\Gamma}_{\mathscr{C}}$. The conditional covariance matrix $\boldsymbol{\Gamma}_{\mathscr{C}}$ is found by

$$\boldsymbol{\Gamma}_{\mathscr{C}} = \boldsymbol{\Gamma}_{\mathscr{N}\mathscr{N}} - \boldsymbol{\Gamma}_{\mathscr{N}\mathscr{O}} \boldsymbol{\Gamma}_{\mathscr{O}\mathscr{O}}^{-1} \boldsymbol{\Gamma}_{\mathscr{O}\mathscr{N}} \tag{21}$$

and the skew $\boldsymbol{\sigma}$ is

$$\boldsymbol{\sigma} = \boldsymbol{L}_{\mathscr{C}} \boldsymbol{y} \tag{22}$$

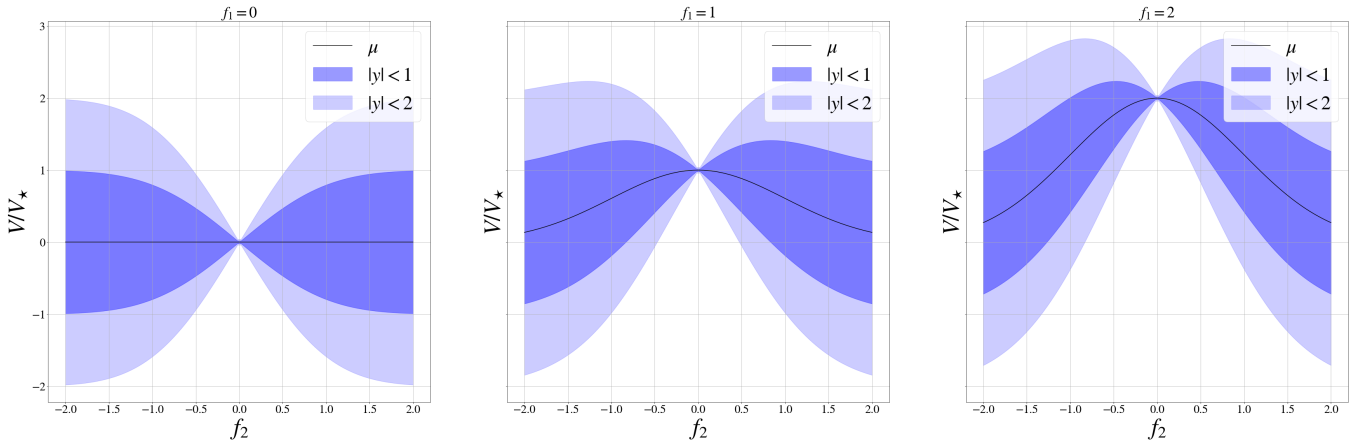

FIG. 1. One-two sigma contour plots of the correlation between two points as a function of their separation in a Gaussian random process. Given $V(\boldsymbol{\phi}_0) = f_1 V_\star$ and simulating $V(\boldsymbol{\phi}_1)$ at some $|\boldsymbol{\phi}_0 - \boldsymbol{\phi}_1| = f_2 s$, the figure shows μ (black line) and the normal distributions for possible variation about μ. When $|f_2|$ is small, the points are close together and V will be highly constrained around $V(\boldsymbol{\phi}_0)$. The influence of V_0 on V_1 decays exponentially as $|f_2|$ grows.

where $\boldsymbol{\Gamma}_{\mathscr{C}} = \boldsymbol{L}_{\mathscr{C}} \boldsymbol{L}_{\mathscr{C}}^T$ is the lower-triangular Cholesky decomposition and $\boldsymbol{y}$ is n randomly sampled standard normal values. As hinted, the randomly generated values are now the sum

$$\boldsymbol{v}_{\mathscr{N}} = \boldsymbol{\mu} + \boldsymbol{\sigma} \tag{23}$$

In the language of probability, $\boldsymbol{y} \sim \mathcal{N}(\boldsymbol{0}, \boldsymbol{1})$ so that $\boldsymbol{\sigma} \sim \mathcal{N}(\boldsymbol{0}, \boldsymbol{\Gamma}_{\mathscr{C}})$ and $\boldsymbol{v}_{\mathscr{N}} \sim \mathcal{N}(\boldsymbol{\mu}, \boldsymbol{\Gamma}_{\mathscr{C}})$.

As a simple example, suppose I sample $V(\boldsymbol{\phi}_0)$ to be $f_1 V_\star$ and I seek to generate $V(\boldsymbol{\phi}_1)$ in which $|\boldsymbol{\phi}_0 - \boldsymbol{\phi}_1| = f_2 s$. In this case, the covariance matrix is

$$\boldsymbol{\Gamma} = \begin{bmatrix} V_\star^2 & V_\star^2 \exp(-f_2^2/2) \\ V_\star^2 \exp(-f_2^2/2) & V_\star^2 \end{bmatrix}. \tag{24}$$

Since $n = 1$, the mean is a scalar,

$$\mu = f_1 V_\star \exp\left(- \frac{f_2^2}{2} \right), \tag{25}$$

as is the conditional covariance matrix,

$$\Gamma_{\mathscr{C}} = V_\star^2 \big[1 - \exp(-f_2^2) \big], \tag{26}$$

and the skew,

$$\sigma = y \sqrt{\Gamma_{\mathscr{C}}}. \tag{27}$$

Some one-two sigma contour plots of possible generations of $V(\boldsymbol{\phi}_1)$ are presented in 1. Note that as $|f_2|$ grows, μ trends from $V(\boldsymbol{\phi}_0)$ toward zero, the would-be mean without constraints, and σ moves from zero toward $y V_\star$, another appropriate trend since without constraints $\langle \sigma^2 \rangle = V_\star^2 \langle y^2 \rangle = V_\star^2$. In other words, the value of V_1 is highly constrained around V_0 when $\boldsymbol{\phi}_1$ is close to $\boldsymbol{\phi}_0$, and the constraints weaken as the separation grows.

Constrained random generation of potential information is not restricted to values of V; the covariance matrix $\boldsymbol{\Gamma}$ can handle any $\boldsymbol{\phi}$-derivatives as well. For example, if $\boldsymbol{v} \equiv \text{append}(\boldsymbol{v}_{\mathscr{C}}, \boldsymbol{v}_{\mathscr{N}})$, $v^{(i)}$ is a value of $\partial V / \partial \phi^{(\alpha)}$, and $v^{(j)}$ is a value of V, then

$$\Gamma^{(ij)} = \left\langle \frac{\partial V_i}{\partial \phi_i^{(\alpha)}} V_j \right\rangle = \frac{\partial}{\partial \phi_i^{(\alpha)}} \langle V_i V_j \rangle \tag{28}$$

$$= \left(\frac{\phi_j^{(\alpha)} - \phi_i^{\alpha}}{s^2} \right) \langle V_i V_j \rangle \tag{29}$$

All correlations between first and second derivatives of V follow from this method, albeit with tedious algebra.

B. The Minimum Condition

On its own, the Gaussian random potential is not an interesting inflationary model as it does not naturally spawn minima at exactly $V = 0$. Given some initial $\boldsymbol{\phi}_i$, the equations of motion (5) will evolve the field down the slopes of V, eventually settling it at a minimum. A nonzero energy density at the end of inflation corresponds either to an eternally inflating universe ($V > 0$) or a collapsing universe ($V < 0$). To isolate universes that evolve similarly to our own while retaining the unique properties of the Gaussian random potential, we impose the following $N^2 + N + 1$ conditions on V before the

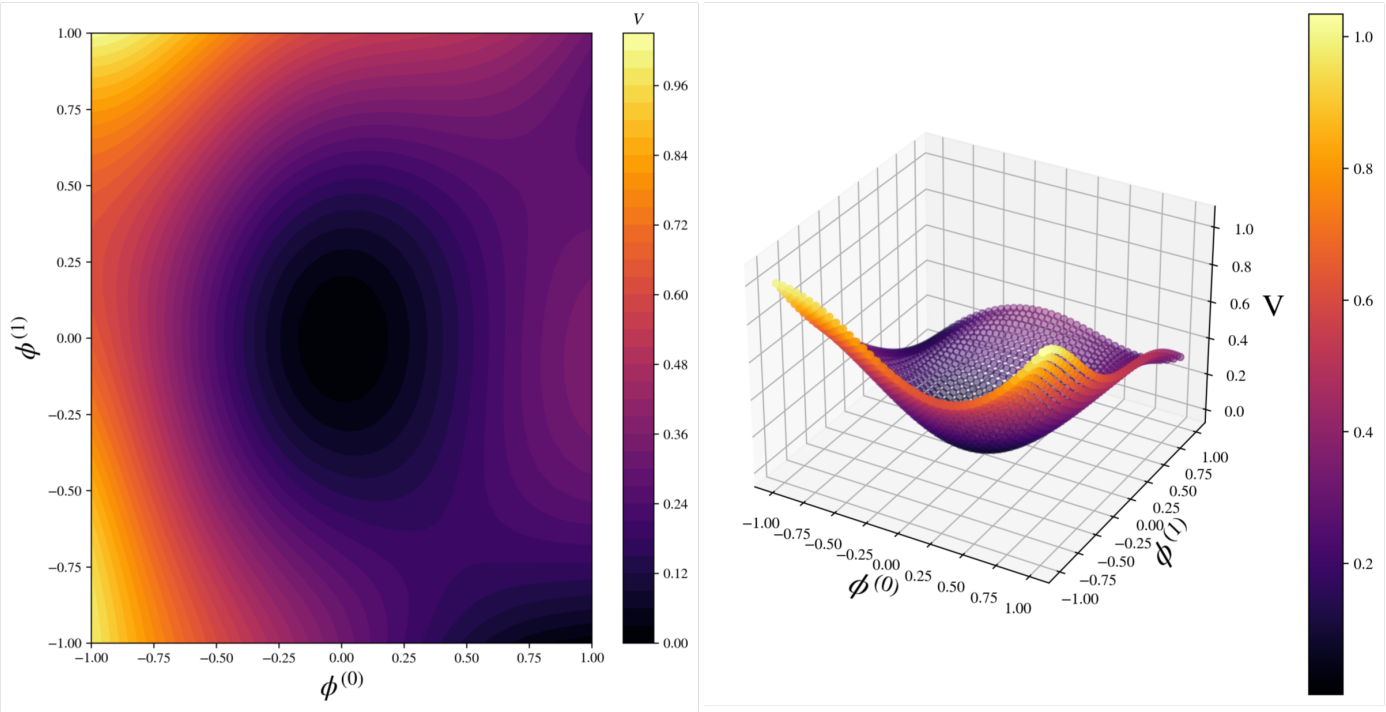

FIG. 2. A 2-dimensional Gaussian random potential V generated at nodes on a 40×40 grid evenly spaced in $\phi^{(0)}, \phi^{(1)}$. *Left*: a "birds-eye view" of the potential isocontours, colored by potential value. *Right*: the same potential function as a traditional 3-D projection, with V as the height. In both panels, the imposed minimum conditions are clearly visible. Note that we do not employ these techniques of generating potential values throughout an entire rectangular domain when solving the trajectory, but do so here for illustrative purposes.

trajectory is solved:

$$V(\mathbf{0}) = 0 \tag{30}$$

$$\frac{\partial V}{\partial \phi^{(\alpha)}}(\mathbf{0}) = 0 \text{ for all } \alpha \tag{31}$$

$$\frac{\partial^2 V}{\partial (\phi^{(\alpha)})^2}(\mathbf{0}) > 0 \text{ for all } \alpha \tag{32}$$

$$\frac{\partial^2 V}{\partial \phi^{(\alpha)} \partial \phi^{(\beta)}}(\mathbf{0}) = 0 \text{ for all } \alpha \neq \beta \tag{33}$$

These conditions ensure that the potential is zero, flat, and concave up at the origin. More precisely, we want the Hessian $\boldsymbol{H}$ to be positive-definite at the origin. Since there are no preferable locations in a Gaussian random field, we could have chosen any location for the minimum, but chose the origin for convenience. Constraints (32) and (33) are equivalent to diagonalizing $\boldsymbol{H}$ and forcing its diagonal elements to be positive. Physically, we reorient our axes to align with the principal directions of curvature. This is a surefire method of enforcing that simulations with $\boldsymbol{\phi}_i$ in the neighborhood of the origin evolve a physically interesting path.

III. COMPUTATIONAL PROCESS

We developed the `bushwhack` code to solve the equations of motion for the inflaton field in an N-dimensional Gaussian random potential. Careful measures were implemented to simplify and compress data related to the random generation of V, the most computationally intensive feature, in hopes of achieving simulations with higher N.

A. The Program

Figure 3 shows the general progression of the `bushwhack` program, from the input of initial conditions to the output information about predicted observable quantities. We detail each step below.

Supply initial conditions. The first step is to fix the parameters s, $V_\star$, and N of the potential, and the initial conditions required for solving the differential equations (5). Since the $V = 0$ minimum, to which we expect the field to evolve at the end of inflation, will be seeded at the origin $\boldsymbol{\phi} = \mathbf{0}$, it is only necessary to supply $\phi_i \equiv |\boldsymbol{\phi}_i|$ instead of N vector components. Once ϕ_i is given, $\boldsymbol{\phi}_i$ is randomized in the N-dimensional shell of that radius. This randomization is necessary to collect a

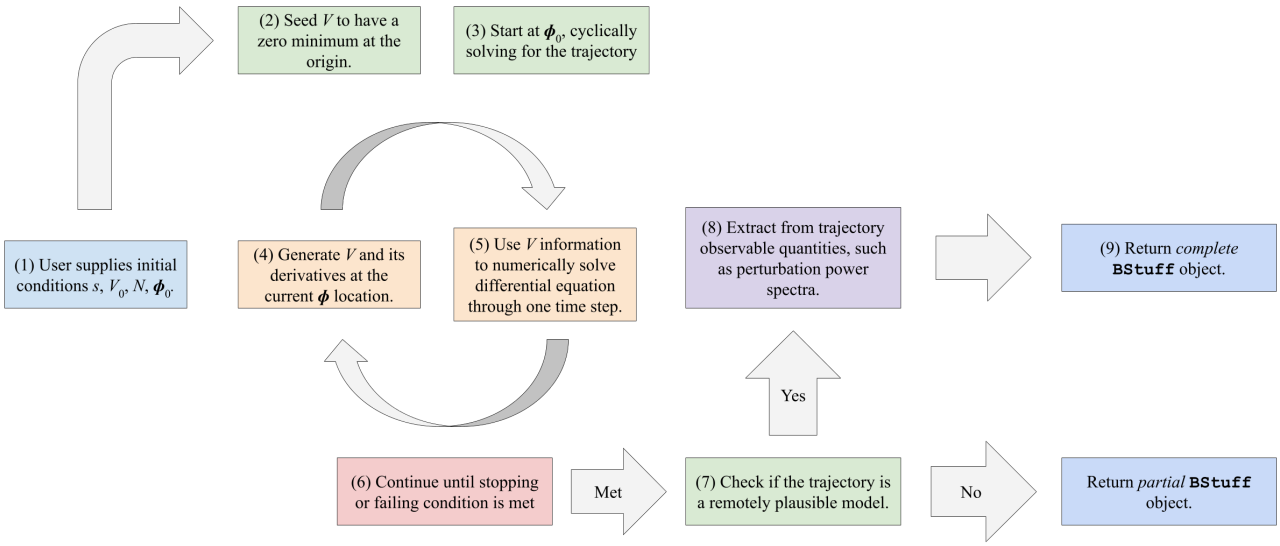

FIG. 3. Flowchart for `bushwhack` code illustrating the chronology of the computational process involved in solving for the trajectory and extracting observable quantities.

representative sample of trajectories for potentials with a given parameter set; forcing $\boldsymbol{\phi}_i = (\phi_i, 0, 0, \ldots, 0)$, for instance, would yield paths which always start along a principal axis of curvature given our method for seeding minima in Section II B. Recall that $\dot{\boldsymbol{\phi}}$ need not be supplied, since its value will be automatically determined by V_i and $\nabla_{\boldsymbol{\phi}} V_i$ via equation (9).

Seed the minimum. Before solving for a trajectory, the code enforces conditions (30)—(33) to ensure subsequent potential generation yields physically plausible solutions. In particular, condition (32) is imposed by randomly simulating N independent second derivative values, taking their absolute values to force them positive, and storing them as the diagonals of the Hessian of V at the origin. At this step, many arrays are initialized such as $\boldsymbol{\Gamma}$, $\boldsymbol{v}$, $\boldsymbol{\phi}$, and $d\boldsymbol{\phi}/dN_e$. The imposed constraints at the origin will remain the first $N^2 + N + 1$ elements of $\boldsymbol{v}$ throughout the simulation and constrain the rest of the potential via a corresponding upper-left block of $\boldsymbol{\Gamma} = \langle \boldsymbol{v}\boldsymbol{v}^T \rangle$.

Simulate—solve cycle. Beginning at $\boldsymbol{\phi}_i$, $N + 1$ data points are randomly generated, V_i and $\nabla_{\boldsymbol{\phi}} V_i$. Those values are then substituted in equation (5) and the field is solved numerically through one time step to $\boldsymbol{\phi}_{i+1}$ via a fourth-order Runge-Kutta solution algorithm. Then V_{i+1} and $\nabla_{\boldsymbol{\phi}} V_{i+1}$ are generated and so continues the "simulate—solve cycle". At any given time step, the potential is generated exactly along the path evolution of $\boldsymbol{\phi}$, constrained by all previously generated data stored in $\boldsymbol{\Gamma}$. In the language of Section II A, old constrains compile into $\boldsymbol{\Gamma}_{\mathscr{O}\mathscr{O}}$, which can get very large as the simulation goes on, while $\boldsymbol{\Gamma}_{\mathscr{N}\mathscr{N}}$ remains an $(N + 1) \times (N + 1)$ square representing new potential and gradient values at the current position.

Stopping conditions. Multiple stopping conditions are monitored at every time step to supervise the evolution of $\boldsymbol{\phi}$. The first slow-roll parameter, ϵ, turns out to be an excellent indicator of the end of inflation. $\epsilon(t_i)$ is a small fraction of unity, but $\epsilon \uparrow 1$ as $\boldsymbol{\phi}$ accelerates into the minimum at the origin. Additionally, we define the "inwardness" parameter ι as the alignment between the slopes of V and the minimum at any given location, or

$$\iota(\boldsymbol{\phi}) \equiv \hat{\nabla_{\boldsymbol{\phi}}} V \cdot \hat{\boldsymbol{\phi}}. \tag{34}$$

where hats represent unit vectors. If $\iota < 0$ at any point during the simulation, then V is sloping away from the origin and it is extremely unlikely that $\boldsymbol{\phi}$ will converge to the $V = 0$ minimum. As a last resort, V itself is monitored. If $V < 0$ at any point, then $\boldsymbol{\phi}$ is in the process of converging to a negative (and, therefore, unphysical) minimum away from the origin. All three conditions—$\epsilon \uparrow 1$, $\iota \downarrow 0$, and $V \downarrow 0$—serve to halt the simulate—solve cycle at the precise moment when either inflation ends or the evolution goes awry. The accumulated data is then bunched into an object of original class `BStuff` and sent off for analysis. `BStuff` objects have attributes that detail every $\boldsymbol{\phi}$ location in the trajectory, as well all information about the potential, constraints, inflation, and stopping conditions

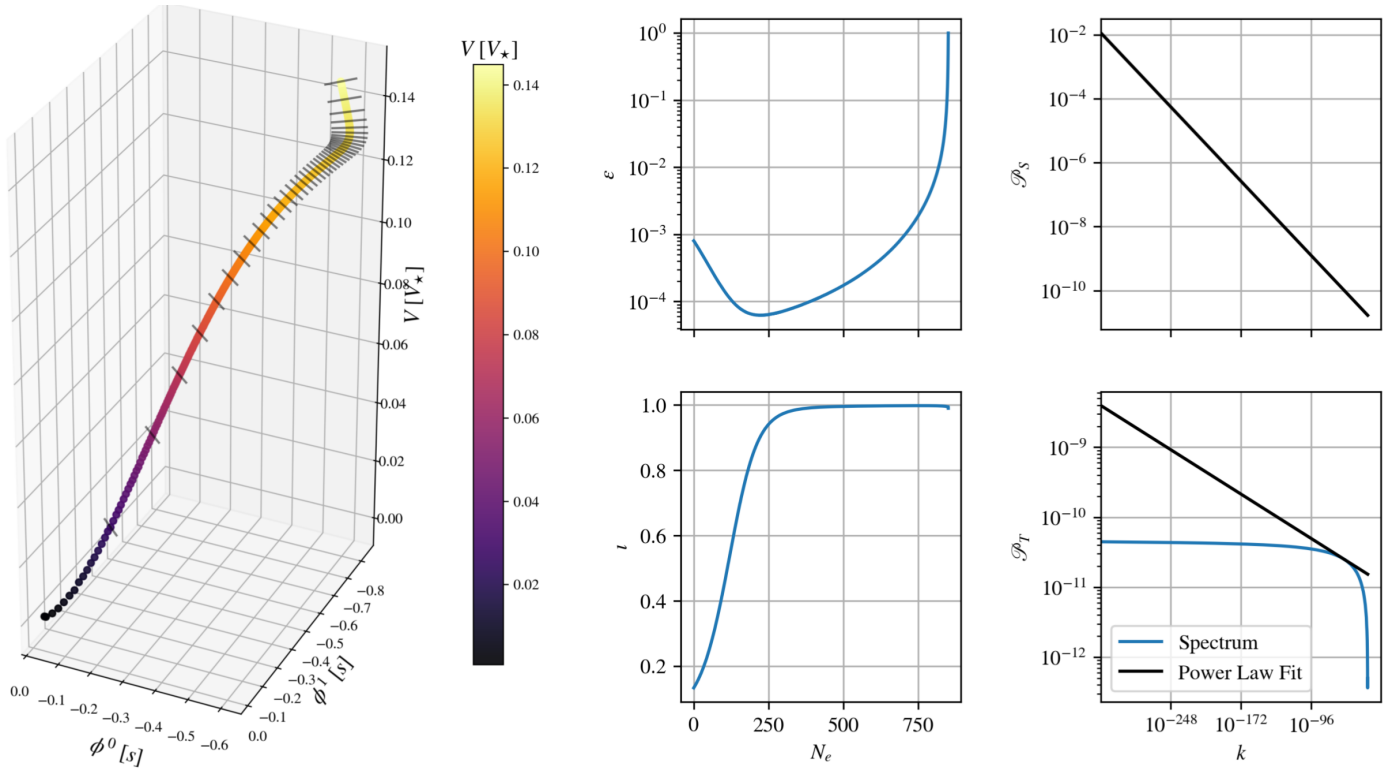

FIG. 4. A sample trajectory in a randomly generated $N = 2$ dimensional Gaussian random field with coherence scale $s = 30$ and energy scale $V_\star = 5 \cdot 10^{-9}$ and some extracted observable quantities. *Left*: discrete points of the path evolution of $\boldsymbol{\phi}$ from some initial $\phi(t_i) = s$ to the end of inflation. The potential value at each point in the evolution is represented on the vertical axis and colored. A line perpendicular to $\nabla_\phi V$ is drawn through every twentieth point. Notice how $\boldsymbol{\phi}$ settles to the minimum seeded at the origin in late times, as desired. *Right*: the left column plots two stopping parameters as a function of number of e-folds. Notice how ϵ accelerates to 1, immediately halting integration. The inwardness parameter ι is never triggered because it never dips below zero. The right column plots two power-law fits to matter (top) and tensor (bottom) power spectra. $\mathscr{P}_S(k)$ does not have an analytic form, so only the fit is shown, while both the analytic form and the fit of $\mathscr{P}_T(k)$ are shown. Note that the approximation is only valid in the neighborhood of $k_0 = 0.05$ Mpc$^{-1} \approx 1.31 \cdot 10^{-58}\, l_{Pl}^{-1}$.

at those locations.

Plausibility check. Once the equations of motion are solved, `bushwhack` makes an effort to determine whether the solution is a remotely plausible representative of our own universe. The verifying questions that the code asks are:

1. Did the solution fail by diverging? In other words, was $\iota(\boldsymbol{\phi}_e) < 0$? If so, do not analyze further. If not, proceed to the next check.

2. Did the solution fail by submerging? In other words, was $V(\boldsymbol{\phi}_e) < 0$? If so, do not analyze further. If not, proceed to the next check.

3. Did the solution accumulate enough inflation? In other words, was $N_e(t_e) \geq 55$? If so, this solution is plausible enough and observable quantities can be extracted. If not, do not analyze further.

Even if the solution fails a plausibility check, the available information is bunched and outputted as an partial `BStuff` object for further manual analysis.

Extract observables. If a trajectory is found to converge to the origin with enough inflation, observable quantities A_S, n_S, A_T, n_T, and r are extracted via methods detailed in Section I B. To sample the matter power spectrum, note from (11) that it is now required to know the second derivatives of V along the path, so those are simulated sparsely along the path using $\boldsymbol{\Gamma}$. It is worth emphasizing here that even with the same set of potential parameters and initial conditions on the trajectory, infinitely different random potentials and trajectories are possible, each of which yield different power spectra. It is only through repeated trials that we compile the *statistical* predictions of observable quantities from a certain parameter set. Visuals of some of the many quantities related to the trajectory and extracted observables are presented in Figure 4.

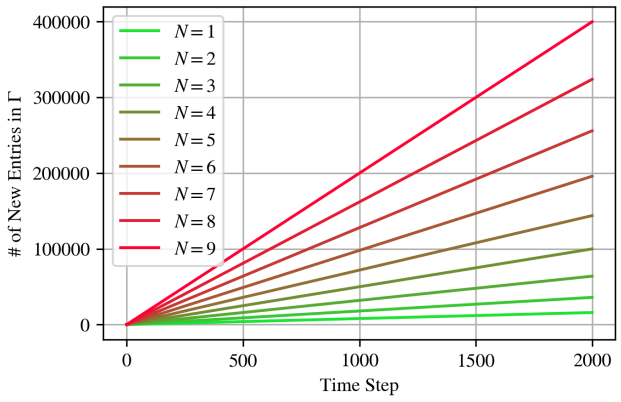

FIG. 5. Several lines indicating the number of new entries required to populate $\mathbf{\Gamma}$ at a certain time step. Since $\mathbf{\Gamma}$ is symmetric, the number of independent correlation functions that need to be calculated is about half the number of new entries.

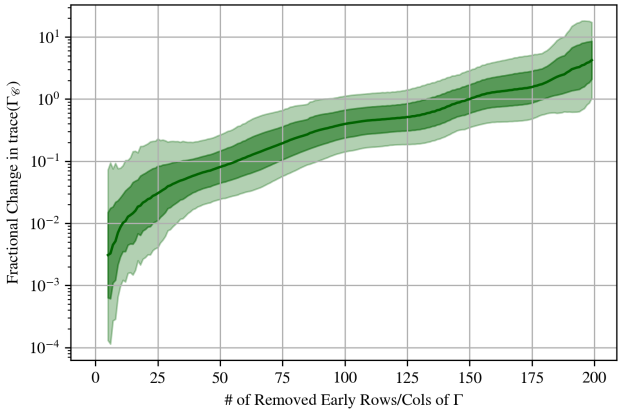

FIG. 6. Constraining power lost from the covariance matrix $\mathbf{\Gamma}$ as a function of ignored information. As more information is removed (higher values on the horizontal axis), the constraints on a new potential value become more relaxed (the conditional covariance matrix $\mathbf{\Gamma}_{\mathscr{C}}$ increases). However, the constraining power of $\mathbf{\Gamma}$ is retained even with many rows and columns removed. Lighter greens show one and two-sigma standard deviations from the mean of several random $N = 2$ simulations.

B. Algorithmic Data Compression

Even when V is simulated only at points along the path evolution of $\boldsymbol{\phi}$, the covariance matrix $\mathbf{\Gamma}$ can become large and ill-conditioned. To illustrate, follow Section II A and suppose that $\boldsymbol{v}_{\mathscr{O}}$ contains all previously generated V values and derivatives, and we seek $\boldsymbol{v}_{\mathscr{N}}$. $\boldsymbol{v}_{\mathscr{O}}$ has length $(N+1)T$, where N is the dimension of V and T is the total number of previous time steps. $\boldsymbol{v}_{\mathscr{N}}$ has length $N+1$. The number of new entries in $\mathbf{\Gamma} = \langle \boldsymbol{v}\boldsymbol{v}^T \rangle$ is

$$\text{entries} = (N+1)^2(T+1)^2 - (N+1)^2T^2 \tag{35}$$
$$= (N+1)^2(2T+1). \tag{36}$$

This growth is visualized in Figure 35. Not only must the matrix be populated, operations must be performed on it, such as Cholesky decompositions. With thousands of time steps in a typical simulation, achieving a representative sample of solutions with high N without compression methods is computationally difficult. We present two methods of data compression that can be applied iteratively throughout a simulation to limit the size of $\mathbf{\Gamma}$ and may help to generate $V(\boldsymbol{\phi})$ more efficiently.

1. *"Unprincipled" Forgetting*

The trajectory of $\boldsymbol{\phi}$ evolves smoothly down the slopes of V; at some time step T, the values nearest $\boldsymbol{\phi}_T$ are usually $\boldsymbol{\phi}_{T-1}, \boldsymbol{\phi}_{T-2}$, etc. By Equation (18), V_T and its derivatives are thus most highly constrained by V_{T-1}, V_{T-2}, etc., and their derivatives. Similarly, if $T \gg 0$, then V_T is unlikely to be highly constrained by early data. It is worth asking: how much of the information contained in $\mathbf{\Gamma}$ contributes a non-negligible constraint on new data?

Consider following the process as described in Section III A to solve for a random $N = 2$ trajectory up through $T-1$ time steps, then seeking to randomly generate the potential value at $\boldsymbol{\phi}_T$. For simplicity, we only consider values of V and not its derivatives in this trajectory. The constraining power of $\mathbf{\Gamma}$ is quantified by the sum of the eigenvalues (i.e., the trace) of $\mathbf{\Gamma}_{\mathscr{C}}$: *higher* values of $\text{Tr}(\mathbf{\Gamma}_{\mathscr{C}})$ correspond to *looser* constraints (higher variance in generated points). Consider removing rows/columns of $\mathbf{\Gamma}$ corresponding to early data, V_i, V_1, V_2 etc., one at a time and recomputing some $\tilde{\mathbf{\Gamma}}_{\mathscr{C}}$ after each removal. In Figure 6, it is shown that when $T = 200$, about 60 early rows/columns of $\mathbf{\Gamma}$ can be deleted before $\text{Tr}(\tilde{\mathbf{\Gamma}}_{\mathscr{C}})$ accumulates a fractional change of 10% from $\text{Tr}(\mathbf{\Gamma}_{\mathscr{C}})$, or about 150 rows/columns before the change is 100%. In practice, even if $\text{Tr}(\mathbf{\Gamma}_{\mathscr{C}})$ is doubled, there is usually not a noticeable discontinuity in the random generation of V_T. We leave it to future studies to quantify exactly how much $\mathbf{\Gamma}$ compression is allowable before disruptive changes in potential generation occur. Still, we assert that the removal of early rows and columns of $\mathbf{\Gamma}$ and relying on more recent (nearby) values to constrain the next generated point is a viable method of increasing computational efficiency when solving trajectories with high N or T.

2. *"Principled" Forgetting*

In the previous subsection, we described a method for increasing computational efficiency that involved compressing $\mathbf{\Gamma}$ under the assumption that earlier points weakly constrain newly generated data. This method was labeled "unprincipled" because it involved the

deletion of data (rather than compression) and affected $\mathrm{Tr}(\mathbf{\Gamma}_{\mathscr{C}})$ indirectly. In this section, we describe a "principled" method of compressing $\mathbf{\Gamma}$ that allows for direct control over the portion of trace kept. We leave its implementation in random field inflationary trajectories to future work (see Section **??**).

We seek to compress $\mathbf{\Gamma}$ so as to maximize its constraining power while minimizing its overall size. When $\boldsymbol{v}_{\mathscr{O}}$ gets large, we seek to find a compression matrix $\boldsymbol{A}$ such that

$$\tilde{\boldsymbol{v}}_{\mathscr{O}} = \boldsymbol{A}\boldsymbol{v}_{\mathscr{O}}, \tag{37}$$

where $\tilde{\boldsymbol{v}}_{\mathscr{O}}$ is a smaller, compressed version of $\boldsymbol{v}_{\mathscr{O}}$. We can transform blocks of $\mathbf{\Gamma}$ into compressed forms as

$$\tilde{\mathbf{\Gamma}}_{\mathscr{O}\mathscr{O}} = \langle \tilde{\boldsymbol{v}}_{\mathscr{O}} \tilde{\boldsymbol{v}}_{\mathscr{O}}^T \rangle = \boldsymbol{A}\mathbf{\Gamma}_{\mathscr{O}\mathscr{O}}\boldsymbol{A}^T \tag{38}$$

$$\tilde{\mathbf{\Gamma}}_{\mathscr{N}\mathscr{O}} = \langle \tilde{\boldsymbol{v}}_{\mathscr{N}} \tilde{\boldsymbol{v}}_{\mathscr{O}}^T \rangle = \mathbf{\Gamma}_{\mathscr{N}\mathscr{O}}\boldsymbol{A}^T \tag{39}$$

$$\tilde{\mathbf{\Gamma}}_{\mathscr{C}} = \mathbf{\Gamma}_{\mathscr{N}\mathscr{N}} - \tilde{\mathbf{\Gamma}}_{\mathscr{N}\mathscr{O}}\tilde{\mathbf{\Gamma}}_{\mathscr{O}\mathscr{O}}^{-1}\tilde{\mathbf{\Gamma}}_{\mathscr{O}\mathscr{N}}. \tag{40}$$

As mentioned previously, *lower* values of $\mathrm{Tr}(\mathbf{\Gamma}_{\mathscr{C}})$ correspond with *tighter* constraints on new potential generation. Thus, to maximize the constraining power of $\tilde{\mathbf{\Gamma}}$, we need to reduce $\mathrm{Tr}(\tilde{\mathbf{\Gamma}}_{\mathscr{C}})$ by maximizing the trace of its latter term,

$$\tau \equiv \mathrm{Tr}(\tilde{\mathbf{\Gamma}}_{\mathscr{N}\mathscr{O}}\tilde{\mathbf{\Gamma}}_{\mathscr{O}\mathscr{O}}^{-1}\tilde{\mathbf{\Gamma}}_{\mathscr{O}\mathscr{N}}) \tag{41}$$

$$= \mathrm{Tr}(\mathbf{\Gamma}_{\mathscr{N}\mathscr{O}}\boldsymbol{A}^T(\boldsymbol{A}\mathbf{\Gamma}_{\mathscr{O}\mathscr{O}}\boldsymbol{A}^T)^{-1}\boldsymbol{A}\mathbf{\Gamma}_{\mathscr{O}\mathscr{N}}) \tag{42}$$

It is straightforward to show that τ only depends on the row space of $\boldsymbol{A}$, so we are free to impose the additional constraint that the rows of $\boldsymbol{A}$ be orthonormal with respect to $\mathbf{\Gamma}_{\mathscr{O}\mathscr{O}}$.

$$\boldsymbol{A}\mathbf{\Gamma}_{\mathscr{O}\mathscr{O}}\boldsymbol{A}^T = \mathbf{1} \tag{43}$$

This constrained maximization problem leads to

$$\boldsymbol{A}\mathbf{\Gamma}_{\mathscr{N}\mathscr{O}}\mathbf{\Gamma}_{\mathscr{O}\mathscr{N}} = \mathbf{\Lambda}\boldsymbol{A}\mathbf{\Gamma}_{\mathscr{O}\mathscr{O}} \tag{44}$$

where $\mathbf{\Lambda}$ is a matrix of Lagrange multipliers. We can once again take linear combinations of the rows of $\boldsymbol{A}$ to diagonalize $\mathbf{\Lambda}$. Now, each row $\boldsymbol{a}$ of $\boldsymbol{A}$ is a solution to the generalized eigenvalue problem

$$\mathbf{\Gamma}_{\mathscr{N}\mathscr{O}}\mathbf{\Gamma}_{\mathscr{O}\mathscr{N}}\boldsymbol{a} = \lambda\mathbf{\Gamma}_{\mathscr{O}\mathscr{O}}\boldsymbol{a}. \tag{45}$$

Since $\tau = \sum_i \lambda_i$, the optimal compression matrix will comprise some number of rows corresponding to the largest eigenvalues so that the size of $\tilde{\mathbf{\Gamma}}_{\mathscr{O}\mathscr{O}}$ is much less than $\mathbf{\Gamma}_{\mathscr{O}\mathscr{O}}$ and $\tau \approx \mathrm{Tr}(\mathbf{\Gamma}_{\mathscr{N}\mathscr{O}}\mathbf{\Gamma}_{\mathscr{O}\mathscr{O}}^{-1}\mathbf{\Gamma}_{\mathscr{O}\mathscr{N}})$. Significant compression may be possible with this method, as the density of data points required to resolve the path evolution of $\boldsymbol{\phi}$ is often greater than what is necessary to describe the potential in a local domain. An overdensity of data points leads to many redundant constraints on new potential generation, and thus a high concentration of τ in the very largest eigenvalues.

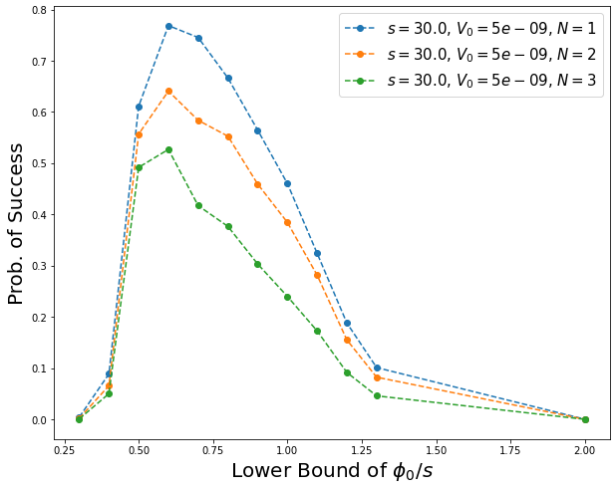

FIG. 7. The probability that a trajectory starting at an initial distance ϕ_i from the origin will both converge and accumulate enough inflation. We did not simulate in the shells between $1.4s$ and $2.0s$ to save time, since the behavior would be well documented by a single data point at $2.0s$. *REDO PLOT IN HIGH DEF + LROMAN FONT + UPDATED X-AXIS*

IV. RESULTS

The `bushwhack` code (see Section III A) was parallelized and implemented with "unprincipled" forgetting (see Section III B 1) for execution on the University of Richmond `SpiderWulf` Supercomputing Cluster. As a preliminary investigation, we choose a some reasonable parameter sets for the generation of V.

$$(s, V_\star^2, N) = (30, 5\cdot 10^{-9}, 1) \tag{46}$$

$$(s, V_\star^2, N) = (30, 5\cdot 10^{-9}, 2) \tag{47}$$

$$(s, V_\star^2, N) = (30, 5\cdot 10^{-9}, 3) \tag{48}$$

The only variable between these sets is N, which may change predictions of observable quantities in nontrivial ways, though varying s and $V_\star$ is worthwhile future work.

To gather a representative sample of trajectories from a given parameter set, we catalogue 1000 simulations with ϕ_i chosen from each of 12 radial ϕ-shells of thickness $0.1s$ from $0.3s$ to $2.1s$. That is, we randomly choose the initial distance from the minimum at the origin to lie within a certain bin (for instance, $\phi_i \in [0.8s, 0.9s]$), then randomly choose the vector location $\boldsymbol{\phi}_i$, all 1000 times in each bin. If $\phi_i < 0.3s$, the trajectory is very unlikely to accumulate enough inflation, and if $\phi_i > 2.1s$, exponentially unlikely to converge to the origin.

A. Weighting Predictions by Success Probabilities

The probability P_S that a trajectory succeeds—converges to the origin with enough inflation—is an

Spectral Quantity	μ_q $(N=1)$	σ_q $(N=1)$	Tension $(N=1)$	μ_q $(N=2)$	σ_q $(N=2)$	Tension $(N=2)$	μ_q $(N=3)$	σ_q $(N=3)$	Tension $(N=3)$
$\log_{10}(A_S)$	-9.4727	0.0909	8.7σ	-9.4875	0.2465	3.3σ	-9.5013	0.2834	2.9σ
n_S	0.96360	0.00205	0.5σ	0.96024	0.02427	0.1σ	0.95786	0.02705	0.2σ
$\log_{10}(A_T)$	-10.404	0.118	N/A	-10.440	0.073	N/A	-10.453	0.089	N/A
n_T	-0.01600	0.00218	N/A	-0.01781	0.00101	N/A	-0.01909	0.00095	N/A
$\log_{10}(r)$	-0.90242	0.07248	1.3σ	-0.92279	0.06822	1.1σ	-0.92139	0.07632	1.0σ

TABLE II. Tabulated results and comparisons. Shown are the weighted means, standard deviations, and tensions with Planck data of various spectral quantities for each parameter set (46)—(48). While A_S predictions exhibit significant tension with Planck data, it may be possible to vary s and $V_\star$ in such a way as to preserve the agreements seen in n_S and r while remedying differences in A_S

interesting function of ϕ_i, plotted at each discrete shell for our chosen parameter sets in Figure 7. To correctly compute the statistical predictions of parameter sets from individual trajectories, it is necessary to weight runs by this function $P_S(\phi_i)$, since there is not an equal likelihood that each trajectory could have naturally occurred. For instance, a successful trajectory with $\phi_i = 2s$ is very unlikely, so its predicted value for r should be a minute contribution to the weighted mean relative to much more commonly successful runs.

In a given parameter set, for some predicted observable quantity q, the weighted mean μ_q considers all shells l as

$$\mu_q = \frac{\sum_l w_l q_l}{\sum_l w_l} \tag{49}$$

where $w_l = P_S(l)$ is a shell weight and q_l is the simple mean of q within l. Similarly, assuming quantity predictions are normally distributed around μ_q, the variance of q is

$$\sigma_q^2 = \frac{\sum_l w_l q_l^2}{\sum_l w_l} - \mu_q^2. \tag{50}$$

B. Power Spectra Predictions

We now present the statistical predictions for observable quantities computed from a Gaussian random inflaton potential with parameters sets (46)—(48). We assume any error resulting from compression methods is accurately represented in the variance of the outputted spectral quantities. First, we examine Figure 8, which plot weighted, normalized histograms for each of A_S, n_S, A_T, n_T, and r for each parameter set, colored by initial condition. A few observations to note:

- Changing N does not significantly affect the mean or variance of any quantity. Future work into higher N is required to confirm that these quantities are insensitive to the dimension of V.
- Quantity distributions within ϕ_i shells are not necessarily the same as the weighted distributions over entire parameter sets. This is especially apparent in the low ϕ_i regime (darker blues); secondary peaks are observed in distributions of A_T and n_T (and, by proxy, r) that are almost completely void of predictions from high ϕ_i simulations.
- Predicted mean values are in variable tension with Planck observations, detailed in Table II. For example, A_S is lower than the Planck prediction for all $N = 1, 2, 3$, while n_S predictions are tightly distributed around the accepted value.
- Distributions roughly normal, but some (in particular n_S and A_T) have slight negative skewness. Thus, the variance may not be the best metric of statistical spread for each quantity.

The predictions visualized in each histogram are quantified in Table II. We also present some spectral quantities against each other as scatterplots (colored, again, by ϕ_i) and Gaussian kernel density estimations (KDEs) in Figure 9. These panels further emphasize a few points:

- The scatterplots do not incorporate weights into their visuals, so the lack of resemblance to a multivariate normal distribution is apparent. Even the appropriately weighted KDEs exhibit curving, nontrivial relationships between quantities.
- The starting location ϕ_i is a highly relevant initial condition for trajectories in Gaussian random potentials. Different ϕ_i bins predict quantities clustered in different regions of the scatterplots. Deep blues (low ϕ_i) and bright yellows (high ϕ_i) show interesting differences from the bulk of the distribution and, even though they are de-weighted to near-negligible contributions, may become of interest with anthropic principle arguments.
- While a majority of the weight goes to tighter regions (as seen in the KDEs), the Gaussian random potential admits many dramatic outliers, making the model all the more interesting and adaptable to modern constraints.

In total, there are ten different combinations of quantities for each of $N = 1, 2, 3$ that could be shown as rows

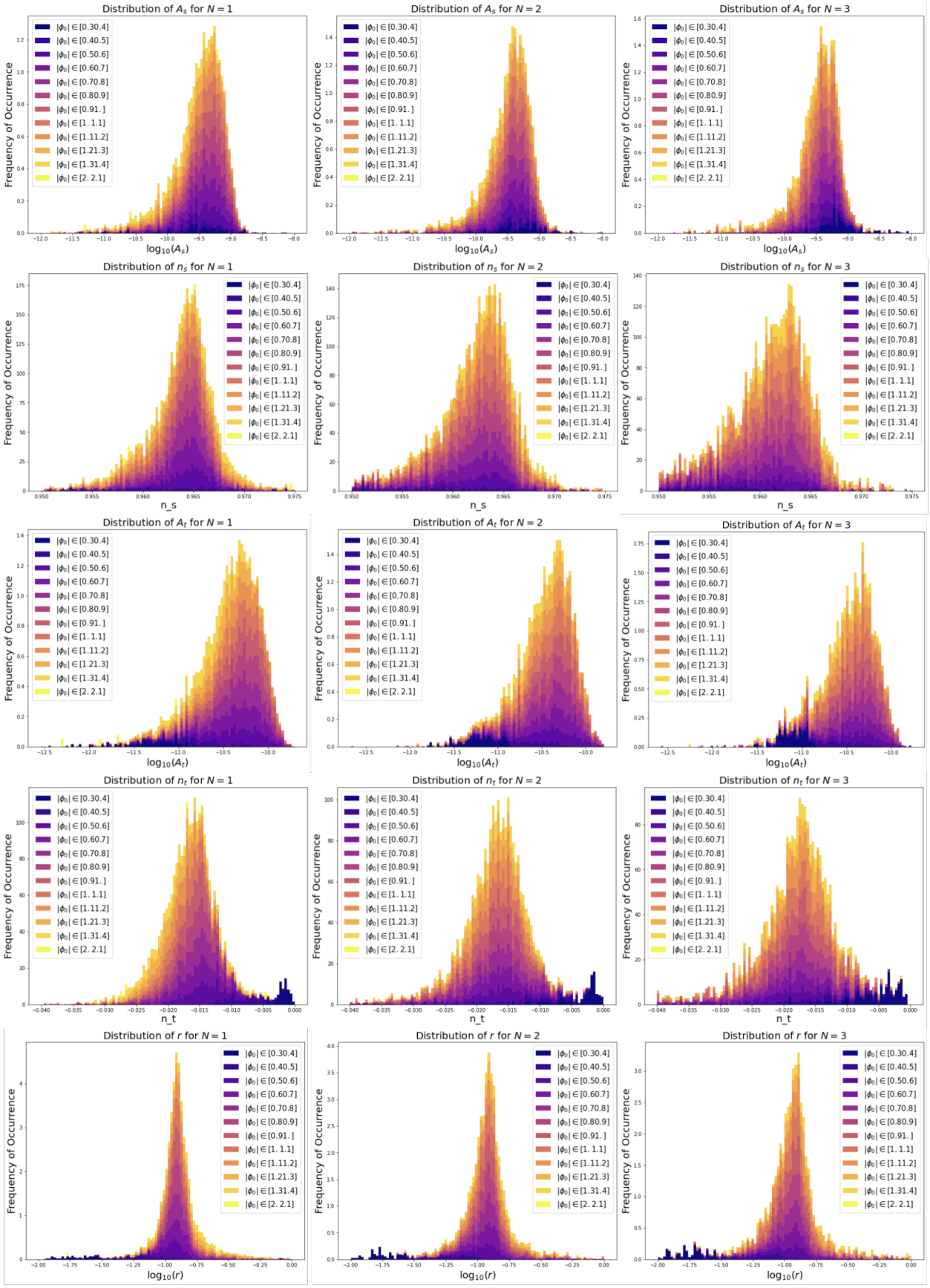

FIG. 8. Weighted histograms of observable quantities A_S, n_S, A_T, n_T, and r. Different colors on each histogram correspond to different initial positions ϕ_i. Each row of plots corresponds to a particular spectral quantity and each column to a parameter set. Horizontal axes are the same along each row.

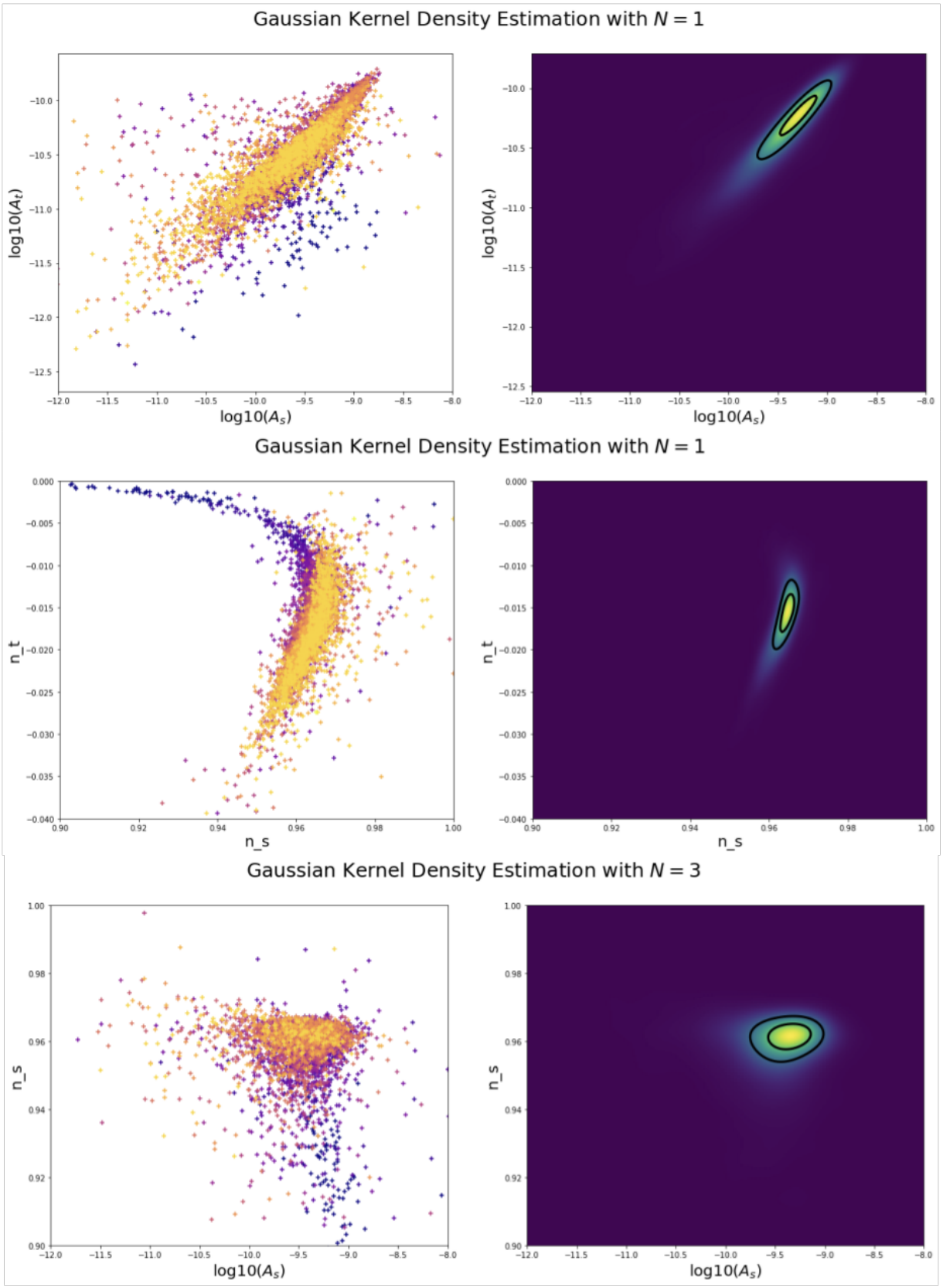

FIG. 9. Gaussian kernel density estimations (KDEs) of scatter-plotted predictions for perturbation spectra. Each cross on the scatter plots corresponds to the prediction of one individual trajectory. The colors of crosses are identical to those in Figure 8. About 11000 individual points are plotted, but many are obscured by points plotted slightly later. The KDEs express the density of the points on the scatter plot. The closed black curves indicate the areas enclosing 68% (inner) and 95% (outer) of the weighted distribution of data.

in Figure 9, but the chosen three are especially demonstrative and enlightening.

V. CONCLUSIONS

We have presented a method for exploration into N-dimensional inflationary models in which the inflaton potential is realized via a Gaussian random process. Information about the potential is not computed throughout a volume, but efficiently generated along the path evolution of the inflaton field. Even still, the covariance matrix of constraints $\mathbf{\Gamma}$ can grow large and unwieldy, as it must track N first derivatives and N^2 second derivatives at each time step for complete precision. We propose two methods of compression, "unprincipled" and "principled" forgetting, that may help to ease the computational intensity by exploiting weak or redundant constraints within $\mathbf{\Gamma}$. We implement unprincipled forgetting steps into our differential equations solver and compile thousands of simulations to characterize the predictions of Gaussian random potentials with three particular parameter sets. We list our main conclusions below:

- The Gaussian random potential a highly versatile inflationary model with a rich volume of promising parameter space. Parameters s, $V_\star$, N, and ϕ_i each change the statistical predictions for perturbation spectra in unique ways. Some parameter sets (such as (46)—(48)) have been demonstrated to accurately predict a number of spectral quantities in Figures 8 and 9.
- Algorithmic data compression allows for the possibility of significantly (*SPECIFY*) more efficient generation of V in high-N regimes. Unprincipled forgetting is limited in that it relies on the assumption that earlier data contributes weaker constraints on new generation and less rigorous in that it involves the deletion of data rather than compression. Principled forgetting methods, if implemented efficiently, could remedy these issues.

A. Future Work

This project could be further explored in a number of ways, ranked below by priority.

1. *Explore parameter space.* Carry out a large number of simulations with different parameter sets which vary s and $V_\star$ in addition to N. These supplemental runs could quantify the degree to which the Gaussian random potential model is able to accurately reproduce modern constraints on primordial power spectra.

2. *Implement principled forgetting.* Unprincipled forgetting offers significant speed increases, but at the expense of rigorous algorithmic data compression. Principled forgetting methods detailed in Section III B 2 have the capacity to provide enormous compression to $\mathbf{\Gamma}$, possibly enough to efficiently explore string-theory-esque models with $N \sim 100$.

3. *Incorporate other observables.* The spectral quantities computed from our trajectories are but a subset of the independent quantities constrained by modern observations. Incorporating quantities such as the non-Gaussianity of the CMB could further verify whether the Gaussian random potential is a plausible inflationary model of our universe.

4. *Translate to other languages.* The `bushwhack` code is currently written in Python, but could be optimized by translating to more efficient languages such as C or FORTRAN.

ACKNOWLEDGEMENTS

This project was supported by two Summer Research Fellowships from the University of Richmond School of Arts & Sciences from May 2019 to July 2020. Simulations were run on the University of Richmond `SpiderWulf` Supercomputing Cluster.

REFERENCES

[1] Y. Akrami et al. "Planck2018 results". In: *Astronomy Astrophysics* 641 (Sept. 2020), A10. ISSN: 1432-0746. DOI: 10.1051/0004-6361/201833887. URL: http://dx.doi.org/10.1051/0004-6361/201833887.

[2] D. Langlois. "Inflation and Cosmological Perturbations". In: *Lecture Notes in Physics* (2010), pp. 1–57. ISSN: 1616-6361. DOI: 10.1007/978-3-642-10598-2_1. URL: http://dx.doi.org/10.1007/978-3-642-10598-2_1.

[3] Layne C. Price et al. "MULTIMODECODE: an efficient numerical solver for multifield inflation". In: *Journal of Cosmology and Astroparticle Physics* 2015.03 (Mar. 2015), pp. 005–005. ISSN: 1475-7516. DOI: 10.1088/1475-7516/2015/03/005. URL: http://dx.doi.org/10.1088/1475-7516/2015/03/005.